AIP | Applied Physics Letters

Temperature dependent near infrared ultraviolet range dielectric functions of nanocrystalline (Na0.5Bi0.5)1− x Ce x (Ti0.99Fe0.01)O3 films

S. Zhang, J. Z. Zhang, M. J. Han, Y. W. Li, Z. G. Hu, and J. H. Chu

Citation: Applied Physics Letters **104**, 041106 (2014); doi: 10.1063/1.4863417
View online: http://dx.doi.org/10.1063/1.4863417
View Table of Contents: http://scitation.aip.org/content/aip/journal/apl/104/4?ver=pdfcov
Published by the AIP Publishing

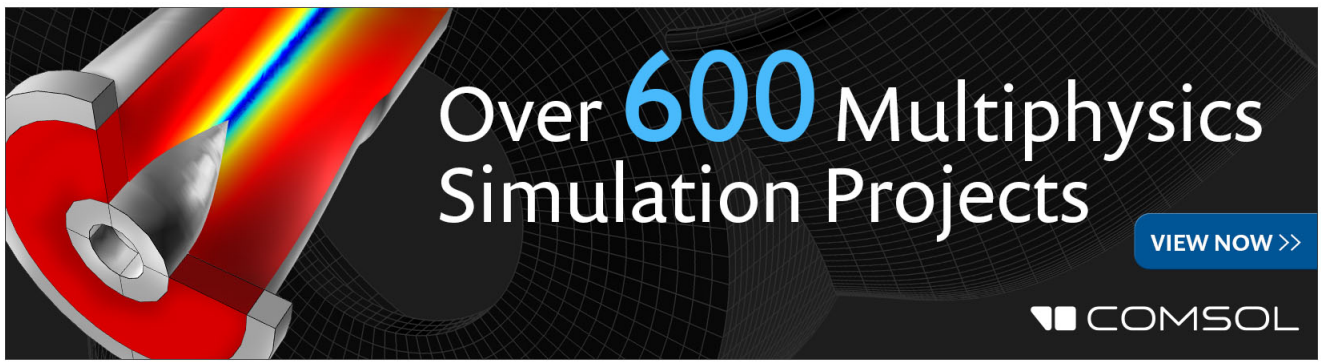

Temperature dependent near infrared ultraviolet range dielectric functions of nanocrystalline $(Na_{0.5}Bi_{0.5})_{1-x}Ce_x(Ti_{0.99}Fe_{0.01})O_3$ films

S. Zhang (张思), J. Z. Zhang (张金中), M. J. Han (韩美杰), Y. W. Li (李亚巍), Z. G. Hu (胡志高),[a] and J. H. Chu (褚君浩)
Key Laboratory of Polar Materials and Devices, Ministry of Education, Department of Electronic Engineering, East China Normal University, Shanghai 200241, China

(Received 20 September 2013; accepted 14 January 2014; published online 28 January 2014)

Optical properties and phase transition of Ce-modified $(Na_{0.5}Bi_{0.5})(Ti_{0.99}Fe_{0.01})O_3$ nanocrystalline films have been investigated by spectroscopic ellipsometry from −70 to 500 °C. Temperature dependent dielectric functions in the photon energy range of 0.6–6.4 eV can be derived by the Tauc-Lorentz model. It was found that the features in dielectric function (ε) showed an abrupt variation near 200 and 340 °C, respectively. The phenomena can be explained by the appearance and/or reversal of polarization. It indicates that ferroelectric (rhombohedral) to paraelectric (tetragonal) phase transition is related to electronic band variation, which is observed by this technique. © *2014 AIP Publishing LLC*. [http://dx.doi.org/10.1063/1.4863417]

Sodium-bismuth titanate $Na_{0.5}Bi_{0.5}TiO_3$ (NBT) was first reported by Smolensky in 1960,[1] whose physical characteristics, particularly dielectric properties and structural phase transitions have been studied.[2,3] NBT is a complex perovskite-structure ferroelectric compound with two different ions at the A site of the ABO_3 structure and relatively high Curie temperature of $T_c = 320$ °C.[4] Unfortunately, NBT exhibits poor piezoelectric coefficients and electric-field-induced strain.[5] Recently, it was found that chemical doping engineering can be used to modify piezoelectric and ferroelectric properties.[6] It was acknowledged that the ionic radii of Ce ion is closer to the A site ion, which can improve ferroelectric properties of $Na_{0.5}Bi_{0.5}TiO_3$- $x$$BaTiO_3$ (NBT-BT) crystals by increasing the remnant polarization and coercive field.[7] On the other hand, the Fe substitution leads to an enhanced piezoelectric coefficient.[8] Besides, NBT has been generally investigated as bulk crystals and ceramics to date,[9,10] but few studies were carried out for films in spite of the fact that they offer excellent ferroelectric and optical properties.[11,12] Moreover, it was discovered that the leakage current can be decreased, and the ferroelectric properties have been improved for (Ce, Fe)-codoped $Na_{0.5}Bi_{0.5}TiO_3$ films.[13] It has been reported that the spectroscopic and electrical data support the above observations.[14] In addition, NBT-based ferroelectric oxides have some advantages for optoelectronic and photovoltaic applications due to environmentally friendly composition and a narrower band gap, as compared to most lead (Pb)-based ferroelectric materials.[13,14] However, temperature dependent physical properties, such as the dielectric function and electronic band structure, are still the open issues. Thus, it is necessary to further investigate optical and phase transition properties of $(Na_{0.5}Bi_{0.5})_{1-x}Ce_x(Ti_{0.99}Fe_{0.01})O_3$ (NBCTFx) films under different conditions in order to develop some promising devices.

Generally, NBT shows unusual dielectric and ferroelectric properties due to its peculiar sequence of phase transitions from the cubic structure at temperatures above 540 °C, to the tetragonal phase in the range of 510–540 °C, afterwards to the rhombohedral structure at temperatures below 300 °C.[15] The correlation between crystal structure and electrical ordering of NBT has been well explained by *in-situ* temperature dependent transmission electron microscope (TEM) study.[16,17] It suggests that the phase transition appears from room temperature ferroelectric (rhombohedral) to paraelectric (tetragonal) phase through an antiferroelectric modulated phase. This modulated phase consists of orthorhombic sheets for a rhombohedral matrix in the temperature range of 200–300 °C. The second phase transition from the orthorhombic to tetragonal phase occurs near 320 °C, which corresponds to the transition from antiferroelectric to paraelectric phase.[16,17] It was also reported that NBT exhibits the rhombohedral symmetry and reveals ferroelectric properties below 200 °C. As for the second temperature range, NBT exhibits paraelectric properties above 340 °C. Note that the phase transition can be found in NBT crystals and ceramics by TEM or X-ray diffraction (XRD).[18,19] However, few reports on the interesting issue have been presented by spectroscopic optical methods. It has been widely accepted that spectral response is representative of the interband and intraband transitions for material studied.

It is generally known that dielectric functions (ε) are directly related to electronic band structure of materials, which are crucial for the design and optimization of optoelectronic devices.[20] Especially, the imaginary part can reflect the electronic transition information of the films. Spectroscopic ellipsometry (SE), which is sensitive to ultrathin films and surfaces, is a nondestructive and powerful technique to investigate optical properties of materials, particularly to measure the thickness and the dielectric functions of a multilayer system simultaneously. SE is widely used to investigate optical properties and microstructures of ferroelectric films on various substrates, which can bring more information on the valence electron structure of the films and help to better understand the features of chemical bonding and structural transformations of the films.

[a]Author to whom correspondence should be addressed. Electronic mail: zghu@ee.ecnu.edu.cn. Tel.: +86-21-54345150. Fax: +86-21-54345119.

In this Letter, optical properties of NBCTFx ($x = 0.08$ and 0.1) films on platinized silicon ($Pt/TiO_2/SiO_2/Si$) substrates have been investigated using variable-temperature SE in the photon energy range of 0.6–6.4 eV (195–2000 nm). The phase transition is revealed in the NBCTFx films with the aid of analyzing the dielectric functions. The anomaly of electronic band transitions during the phase transition has been discussed in detail.

The NBCTFx films on $(111)Pt/TiO_2/SiO_2/Si$ were fabricated by a sol-gel method. The raw materials for the preparation of NBCTFx films were analytically pure bismuth nitrate [$Bi(NO_3)_3 \cdot 5H_2O$, 99%], sodium acetate trihydrate ($CH_3COONa \cdot 3H_2O$, 99%), titanium butoxide {$Ti[O(CH_2)_3CH_3]_4$, 98%}, ferric nitrate ninehydrate [$Fe(NO_3)_3 \cdot 9H_2O$, 98.5%], and cerium nitrate hexahydrate [$Ce(NO_3)_3 \cdot 6H_2O$, 99.9%]. By the corresponding mixing and dissolving, the NBCTFx solutions were 0.3 M, which were taken as precursors for the fabrication. The NBCTFx films were deposited by spin coating onto the $(111)Pt/TiO_2/SiO_2/Si$ substrates at a speed of 4000 rpm for 20 s. Finally, all the films with the thickness of about 180 nm were obtained by a rapid thermal annealing procedure.[14] The XRD results of the NBCTF0.08 and NBCTF0.1 films indicated that all the films are polycrystalline without impurity phases (such as Fe_2O_3 etc.) at room temperature except for the rhombohedral phase (JCPDS card, No. 36-0340) and the detailed results can be found elsewhere.[14] Moreover, the X-ray photoelectron spectroscopy (XPS) measurements suggest that the Ce concentrations are in good agreement with the nominal atomic compositions of $x = 0.08$ and 0.1, respectively.

The surface morphology of the films was examined by atomic force microscopy (AFM) (Digital Instruments Dimension Icon, Bruker). The scale height is 20 nm and the measured area is $1 \times 1\ \mu m^2$. Figures 1(a) and 1(b) show the AFM two-dimensional images of the NBCTFx films. It suggests that the surface morphology presents the similar pattern while the root-mean-square roughness is estimated to 3.2 and 4.1 nm for $x = 0.08$ and 0.10, respectively. The

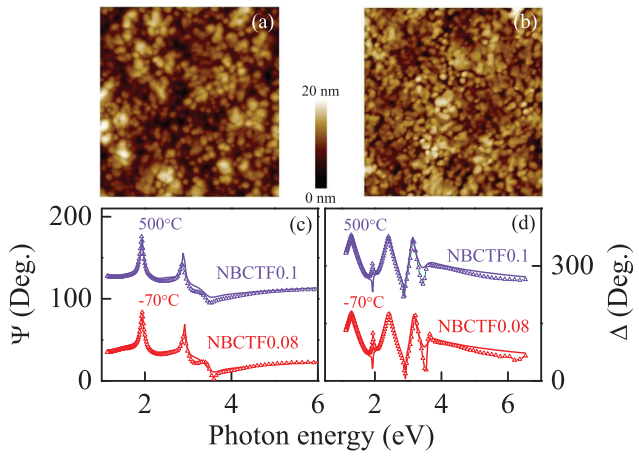

FIG. 1. The AFM two-dimensional images of (a) NBCTF0.08, (b) NBCTF0.1, respectively. Note that the scale height is 20 nm and the measured area is $1 \times 1\ \mu m^2$. Near infrared-ultraviolet experimental (dotted lines) and best-fitted ellipsometric spectra (c) Ψ and (d) Δ of the NBCTF0.08 and NBCTF0.1 films under −70 °C and 500 °C, respectively. Note that the Ψ and Δ spectra of the NBCTF0.1 film are vertically shifted by adding 90 and 200, respectively.

ellipsometric measurements were carried out by a near-infrared-ultraviolet (NIR-UV) SE in the wavelength range of 195–2000 nm (0.6–6.4 eV) with a spectral resolution of 2 nm (V-VASE by J. A. Woollam Co., Inc.). The incident angle was selected to 70° for the films corresponding to the experimental optimization near the Brewster angle of Si. Note that the Pt layer with the thickness of about 150 nm is optically opaque in the photon energy range of 0.6–6.4 eV and its optical constants were taken from Ref. 21. As for the variable temperature measurements, the samples are mounted into an Instec cell and the temperature can be set from −70 to 500 °C with a precision of about ±1 °C. The spectra were analyzed with the WVASE32 software package. Note that the surface roughness obtained by the fitting SE data is slightly larger than the root-mean-square roughness derived from the AFM pictures. It should be emphasized that the NBCTFx films were deposited on $(111)Pt/TiO_2/SiO_2/Si$ substrates with the size of about 2 cm. The measured sample volumes in SE and AFM measurements are obviously diverse due to different incident light spots, which can induce the above discrepancy.

To extract the dielectric functions $[\tilde{\varepsilon}(E) = \varepsilon_1(E) + i\varepsilon_2(E)]$ and other physical parameters of ferroelectric NBCTFx nanocrystalline films, the ellipsometric spectra were explained by a four-layer structure (air/surface rough layer (SRL)/NBCTFx/Pt). It should be emphasized that the fitting reliability mainly depends on the selection of the dielectric function models. The dielectric response of semiconductor/dielectric materials in the frequency region of visible light can result from the interband electronic transitions. There are many dispersion functions expressing the interband transition contributions and a dielectric function derived directly from the band gap theory is desirable for the NBCTFx films. Fortunately, the Tauc-Lorentz (TL) model is a useful model to express the dielectric dispersion of the perovskite systems in the NIR-UV frequency region.[22,23] The standard quantum mechanical or Lorentz calculation for ε_2 (the imaginary part of the complex dielectric function) of a collection of noninteracting atoms has been widely applied in many solid materials from transparent to strong absorption region.[24] The imaginary part can be written as $\varepsilon_2(E) = \frac{A_0 E_n C (E-E_g)^2}{(E^2-E_n^2)^2 + C^2 E^2} \frac{1}{E}$, $(E \geq E_g)$; $\varepsilon_2(E) = 0$, $(E < E_g)$ and the real part is given by the Kramers-Krönig transformation (KKT) $\varepsilon_1(E) = 1 + \frac{2}{\pi} P \int_{E_g}^{\infty} \frac{\xi \varepsilon_2(\xi)}{\xi^2 - E^2} d\xi$. They are depending on the following four parameters: the transition matrix element A_0, the peak transition energy E_n, the broadening term C, and the Tauc gap energy E_g. It should be pointed out that the true band gap is slightly higher than the Tauc gap energy derived from the TL model due to the existence of Urbach tails which are not included in this dispersion model. Nevertheless, a good coincidence was obtained between the experimental and fitted data in the entirely measured photon energy region by using the TL model in the present work [Figures 1(c) and 1(d)]. It indicates that the dielectric function model can reasonably describe the interband transition of the present NBCTFx films. A SRL must be taken into account to exclude surface fluctuation effects from the high-temperature annealing.[25] The dielectric function of the SRL as a mixture of 50% film

TABLE I. Dielectric function parameters using the Tauc-Lorentz oscillator formalism for the NBCTF x films determined from the simulation of ellipsometric spectra in Figure 1. Note that σ is the root-mean-square fractional error. The 90% reliability of the fitting parameters is given with (±).

Samples	NBCTF0.08					NBCTF0.1				
T (°C)	A_0 (eV)	E_g (eV)	E_n (eV)	C (eV)	σ	A_0 (eV)	E_g (eV)	E_n (eV)	C (eV)	σ
−70	670 ± 22	3.00 ± 0.01	3.04 ± 0.06	5.39 ± 0.35	10.5	406 ± 23	3.01 ± 0.01	3.86 ± 0.09	5.11 ± 0.29	8.5
320	669 ± 35	2.99 ± 0.02	3.02 ± 0.08	5.20 ± 0.28	9.8	372 ± 14	3.00 ± 0.01	3.98 ± 0.54	4.48 ± 0.22	7.8
330	669 ± 34	2.99 ± 0.02	3.02 ± 0.08	5.20 ± 0.27	9.6	372 ± 11	3.00 ± 0.01	3.98 ± 0.04	4.48 ± 0.23	7.8
340	669 ± 34	2.99 ± 0.02	3.02 ± 0.08	5.20 ± 0.27	9.6	372 ± 9	3.00 ± 0.01	3.97 ± 0.03	4.48 ± 0.23	7.7
350	668 ± 35	2.99 ± 0.02	3.02 ± 0.08	5.19 ± 0.27	9.4	439 ± 14	2.94 ± 0.01	3.51 ± 0.04	4.87 ± 0.22	7.7
360	668 ± 69	2.98 ± 0.03	3.01 ± 0.16	5.15 ± 0.46	9.4	439 ± 15	2.94 ± 0.01	3.50 ± 0.05	4.87 ± 0.22	7.8
500	660 ± 59	2.93 ± 0.16	2.94 ± 0.10	4.93 ± 0.72	8.9	487 ± 15	2.93 ± 0.01	3.26 ± 0.04	4.59 ± 0.18	7.2

and 50% voids was expressed with the aid of Brüggeman effective medium approximation.[26] The thicknesses (film d_f and surface roughness d_s) of the NBCTF0.08 and NBCTF0.10 films at room temperature are about 171 nm ($d_f = 162 \pm 2$ nm and $d_s = 8.8 \pm 0.4$ nm) and 185 nm ($d_f = 177 \pm 2$ nm and $d_s = 7.9 \pm 3.2$ nm), respectively. To avoid the strong coefficient correlation between the fitting parameters, the values of thicknesses taken from room temperature have been fixed during the fitting calculations at different temperatures. In addition, the root-mean-square fractional error σ is defined by $\sigma^2 = \frac{1}{2J-K}\sum_{i=1}^{J}\left[\left(\frac{\Psi_i^{mod}-\Psi_i^{exp}}{\sigma_{\Psi,i}^{exp}}\right)^2 + \left(\frac{\Delta_i^{mod}-\Delta_i^{exp}}{\sigma_{\Delta,i}^{exp}}\right)^2\right]$, where J is the number of data points and K is the number of unknown model parameters, has been used to judge the quality of the fit between measured and model data.[27]

As an example, the ellipsometric angles Ψ and Δ of the NBCTF0.08 and NBCTF0.1 films at −70 and 500 °C are shown by the dotted lines in Figures 1(c) and 1(d), respectively. The Fabry-Pérot interference patterns due to the finite thickness are observed below the photon energy of about 3.6 eV, indicating that the films are transparent in the photon energy region. The dielectric function of the NBCTFx films can be extracted by fitting the model function to the measured data. The fitted parameter and σ values are summarized in Table I, and the fitted ellipsometric spectra Ψ and Δ are shown by the solid lines in Figures 1(c) and 1(d), respectively. The evaluated dielectric functions of the NBCTF0.08 and NBCTF0.1 films are shown in Figure 2. To clarify the temperature evolution of the dielectric functions, the two parameters were plotted and the correspondingly vertical shifts are also shown in the insets. Interestingly, the obvious temperature effects can be observed. The evolution of ε with the photon energy is a typical optical response behavior of semiconductor materials. The parameter ε_2 increases with the photon energy and approaches the maximum around 5.4 eV, which indicates that a strong optical absorption appears. However, the parameter ε_1 increases with the photon energy and approaches the maximum value around 3.6 eV, which indicates a transition and ascent of absorption edge, as shown in Figures 2(a) and 2(c). Then, the real part of dielectric function decreases towards a higher energy side because of the known Van Hove singularities. It should be emphasized that the maximum values of real and imaginary parts are consistent due to the KKT rule.

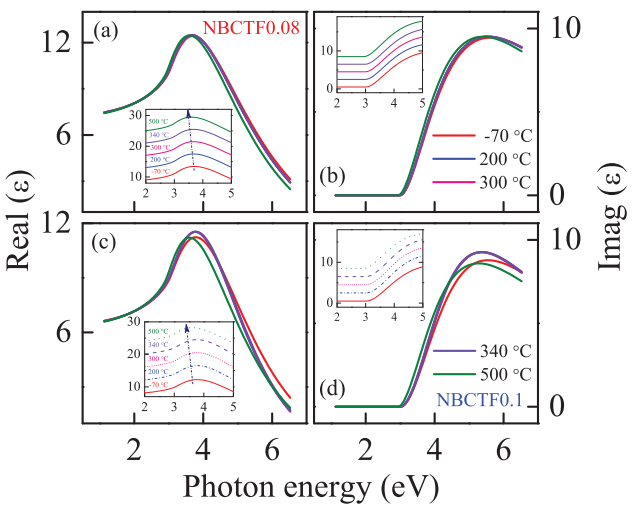

FIG. 2. Evolution of (a)/(c) the real part ε_1 and (b)/(d) the imaginary part ε_2 of the NBCTF0.08 and NBCTF0.1 films with the temperatures. Note that the insets show ε_1 and ε_2 in the photon energy range of 2–5 eV, which are vertically shifted by adding 4 and 2 for each temperature, respectively.

The temperature evolution of ε_1(T) measured in the transparent range with the photon energy of 2.5 eV is shown in Figure 3. A deviation from the low temperature linear behavior ε_1(T) appears at about 200 °C (the shade part "I"). The deviation extends to a temperature region of about 200–340 °C at which the $d\varepsilon_1/dT$ values are changed. Then, ε_1(T) starts to increase abruptly at about 340 °C (the shade part "II"). On the other hand, the optical absorption edge of nanocrystalline NBCTFx films was obtained under different temperatures to get a temperature evolution of the Tauc gap energy E_g. From Figure 4, the parameter E_g of both NBCTF0.08 and NBCTF0.1 films decreases slightly with increasing the temperature below 200 °C. Correspondingly, the parameter d E_g/dT begins to change at 200 °C ("I"). Finally, the Tauc gap E_g of both NBCTF0.08 and NBCTF0.1 films starts to decrease abruptly at about 340 °C ("II"), especially for the NBCTF0.1 film.

The first phase transition from ferroelectric (rhombohedral) to antiferroelectric (orthorhombic) in the polycrystalline NBCTF0.08 and NBCTF0.1 films appears at about 200 °C. Meanwhile, the second phase transition from antiferroelectric (orthorhombic) to paraelectric (tetragonal) is located at about 340 °C with the temperature width of about

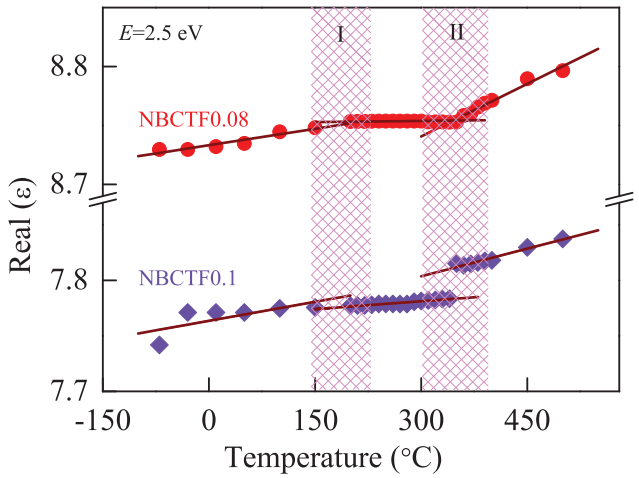

FIG. 3. The real part ε_1 at the photon energy of 2.5 eV as a function of temperature for the NBCTFx films. The shade parts "I" and "II" indicate two different phase transition regions, respectively. Note that the straight lines are used to distinguish the discrepancy.

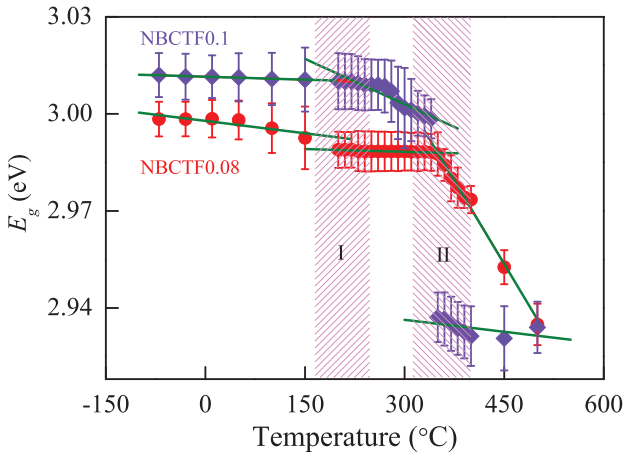

FIG. 4. Tauc gap (E_g) as a function of temperature for the NBCTFx films. Correspondingly, the shade part "I" shows the first phase transition from ferroelectric rhombohedral to antiferroelectric orthorhombic. The shade part "II" presents the second phase transition from antiferroelectric orthorhombic to paraelectric tetragonal. Note that the linear fitting is applied to guide the eyes.

140 °C. Although the physical mechanisms leading to such a behavior are still under investigation, the linear $\varepsilon_1(T)$ behavior can be taken as an experimental indication of the high-temperature paraelectric state in the NBCTFx films. Such a deviation is commonly ascribed to the appearance of charge polarization, which causes a change in the index of refraction via the quadratic electro-optic effect while the structure remains cubic on average.[28–30] The temperature dependence of $\varepsilon_1(T)$ reflects intrinsic states and their variations in the NBCTFx films. The high-temperature phase state is clearly evidenced by the linear increase of ε_1. The observed deviation from the high-temperature linear $\varepsilon_1(T)$ behavior indicates the appearance of local polarization, which is not yet ordered on the long-range scale.[31] The long-range ferroelectric order is established at about 340 °C, as shown in Figure 3. Note that $\varepsilon_1 = n^2 - \kappa^2$, here n is the refractive index and κ is the extinction coefficient. Therefore, the formula $\varepsilon_1 = n^2$ is valid only in the transparent region. It can be concluded that the observed variation trend of $n(T)$ agrees with the behavior of refractive index in NBCTFx nanocrystalline films. Obviously, the inspection of $\varepsilon_1(T)$ can be applied to analyze intrinsic phase transition of oxide films.

From Figure 4, the Tauc gap E_g decreased with increasing the temperature in general, with values are closer to those from NBT single crystals.[32] It is commonly acknowledged that the decrease of the optical band gap with the temperature is due to the electron-phonon interaction and the lattice thermal expansion.[33] With increasing the temperature, the interatomic distance along the direction of their propagation can be changed by the longitudinal phonons,[34] which will further affects the lattice constant and results in the modification of energy band structure. Finally, the phenomena can move the conduction band (CB) downward and the valence band (VB) upward. The VB of NBCTFx films mainly consists of the O_{2p}, $Bi_{6s,6p}$, and Ti_{3d} states in the perovskite type unit and the O_{2p} orbital is strongly hybridized with the Ti_{3d} (O_{2p}-Ti_{3d}), and Bi (O_{2p}-$Bi_{6s,6p}$) orbital below the Fermi level E_F. However, the CB is dominated by Ti_{3d} states, Bi_{6p}, and $Na_{2s,2p}$ with minor contributions from O_{2p} states.[35] Also, there is considerable hybridization between Ti_{3d}, Bi_{6p}, $Na_{2s,2p}$, and O_{2p} in the CB. In the case of Ce-substituted NBTF films, the Ce atoms substitute the partial Bi and Na atoms in the pseudo-perovskite unit. The structure of the films starts to change from rhombohedral to orthorhombic near 200 °C and orthorhombic to tetragonal around 340 °C, which can influence the electronic structure and result in the variation of E_g. The maximum in the real part of the dielectric function of NBCTFx has been revealed at about 3.7 eV. According to the results of first-principles calculations, the interband optical transitions can be derived from prevailingly O_{2p} valence band to the relatively localized Ti_{3d} and Bi_{6p} originated conduction bands.

In summary, the NBCTFx nanocrystalline films ($x = 0.08$ and 0.1) on platinized silicon ($Pt/TiO_2/SiO_2/Si$) substrates by the sol-gel method have been investigated near phase transition region. There is an antiferroelectric modulated phase during the phase transition process. A distinct spectral band for the real part of dielectric function has been revealed in the spectral range of 0.6–6.4 eV with maximum at about 3.7 eV. The critical parameter E_g and dielectric function ε_1 showed an abrupt transformation, indicating abnormal variation of the electronic structure near the phase transition region.

One of the authors (S. Zhang) would like to thank Liping Xu and Pengpeng Jiang for SE measurements and Ting Huang for AFM measurements. This work was financially supported by Major State Basic Research Development Program of China (Grant Nos. 2011CB922200 and 2013CB922300), Natural Science Foundation of China (Grant Nos. 11374097, 61376129, 11074076, and 61106122), Projects of Science and Technology Commission of Shanghai Municipality (Grant Nos. 13JC1402100 and 13JC1404200), the Program for Professor of Special Appointment (Eastern Scholar) at Shanghai Institutions of Higher Learning.

[1]G. A. Smolenski, V. A. Isupov, A. I. Agranovskaya, and N. N. Krainik, Sov. Phys. Solid State **2**, 2651 (1961).
[2]J. Suchanicz and W. S. Ptak, Ferroelectr. Lett. **12**, 71 (1990).
[3]C. S. Tu, I. G. Siny, and V. H. Schmidt, Phys. Rev. B **49**, 11550 (1994).
[4]D. Z. Jin, X. M. Chen, and Z. C. Xu, Mater. Lett. **58**, 1701 (2004).
[5]Y. Hiruma, H. Nagata, and T. Takenaka, J. Appl. Phys. **105**, 084112 (2009).

[6]D. Viehland, J. Am. Ceram. Soc. **89**, 775 (2006).
[7]J. B. Babu, M. He, D. F. Zhang, X. L. Chen, and R. Dhanasekaran, Appl. Phys. Lett. **90**, 102901 (2007).
[8]M. Davies, E. Aksel, and J. L. Jones, J. Am. Ceram. Soc. **94**, 1314 (2011).
[9]A. Q. Jiang and L. D. Zhang, Phys. Rev. B **60**, 9204 (1999).
[10]T. V. Kruzina, V. M. Duda, and J. Suchanicz, Mater. Sci. Eng., B **87**, 48 (2001).
[11]M. L. Zhao, Q. Z. Wu, C. L. Wang, J. L. Zhang, Z. G. Gai, and C. M. Wang, J. Alloys Compd. **476**, 393 (2009).
[12]B. Andriyevsky, J. Suchanicz, C. Cobet, A. Patryn, N. Esser, and B. Kosturek, Phase Transitions **82**, 567 (2009).
[13]C. H. Yang, G. D. Hu, W. B. Wu, H. T. Wu, and F. Yang, Appl. Phys. Lett. **100**, 022909 (2012).
[14]S. Zhang, M. J. Han, J. Z. Zhang, Y. W. Li, Z. G. Hu, and J. H. Chu, ACS Appl. Mater. Interfaces **5**, 3191 (2013).
[15]J. Suchanicz, Ferroelectrics **172**, 455 (1995).
[16]V. Dorcet, G. Trolliard, and P. Boullay, Chem. Mater. **20**, 5061 (2008).
[17]G. Trolliard and V. Dorcet, Chem. Mater. **20**, 5074 (2008).
[18]J. A. Zvirgzds, P. P. Kapostin, J. V. Zvirgzde, and T. V. Kruzina, Ferroelectrics **40**, 75 (1982).
[19]J. Suchanicz and J. Kwapulinski, Ferroelectrics **165**, 249 (1995).
[20]Z. H. Duan, Z. G. Hu, K. Jiang, Y. W. Li, and G. S. Wang, Appl. Phys. Lett. **102**, 151908 (2013).
[21]E. D. Palik, *Handbook of Optical Constants of Solids* (Academic Press, New York, 1985).
[22]S. B. Anooz, J. Schwarzkopf, R. Dirsyte, E. Ehrstein, P. Petrik, A. Kwasniewski, G. Wagner, and R. Fornari, Thin Solid Films **519**, 3782 (2011).
[23]Y. J. Cho, N. V. Nguyen, C. A. Richter, J. R. Ehrstein, B. H. Lee, and J. C. Lee, Appl. Phys. Lett. **80**, 1249 (2002).
[24]G. E. Jellison, Jr. and F. A. Modine, Appl. Phys. Lett. **69**, 371 (1996); **69**, 2137 (1996).
[25]J. Kvietkova, B. Daniel, M. Hetterich, M. Schubert, D. Spemann, D. Litvinov, and D. Gerthsen, Phys. Rev. B **70**, 045316 (2004).
[26]Z. G. Hu and P. Hess, Appl. Phys. Lett. **89**, 081906 (2006).
[27]J. A. Woollam, *Guide to Using WVASE 32* (J. A. Woollam Co., Inc., 2005).
[28]A. S. Bhalla, R. Guo, L. E. Cross, G. Burns, F. H. Dacol, and R. R. Neurgaonkar, Phys. Rev. B **36**, 2030 (1987).
[29]O. Yu. Korshunov, P. A. Markovin, and R. V. Pisarev, Ferroelectr. Lett. **13**, 137 (1992).
[30]P. A. Markovin, W. Kleemann, R. Lindner, V. V. Lemanov, O. Yu. Korshunov, and P. P. Syrnikov, J. Phys.: Condens. Matter **8**, 2377 (1996).
[31]M. Tyunina, A. Dejneka, D. Chvostova, J. Levoska, M. Plekh, and L. Jastrabik, Phys. Rev. B **86**, 224105 (2012).
[32]H. W. Zhang, Q. H. Zhang, X. Y. Zhao, X. B. Li, D. Wang, and H. S. Luo, Appl. Phys. Lett. **102**, 202904 (2013).
[33]S. A. Lourenco, I. F. L. Dias, J. L. Duarte, E. Laureto, E. A. Meneses, J. R. Leite, and I. Mazzaro, J. Appl. Phys. **89**, 6159 (2001).
[34]S. Biernacki, U. Scherz, and B. K. Meyer, Phys. Rev. B **49**, 4501 (1994).
[35]M. Zeng, S. W. Or, and H. L. W. Chan, J. Appl. Phys. **107**, 043513 (2010).